Cureus
Part of SPRINGER NATURE

Open Access Case Report

Intraoperative Subcallosal Cingulate Local Field Potential Spectral Analysis During Emotion-Evoking Music in Treatment-Resistant Depression With Multitarget Deep Brain Stimulation: A Case Report

William O. Contreras López [1, 2, 3], Carlos Aníbal Restrepo Bravo [4]

1. Functional Neurosurgery, International Neuromodulation Center NEMOD, Clínica FOSCAL Internacional, Floridablanca, COL 2. Neurosurgery, Hospital Internacional de Colombia, Piedecuesta, COL 3. School of Medicine, Universidad Autónoma de Bucaramanga, Bucaramanga, COL 4. Neurophysiology, Faculty of Health Sciences, Universidad CES, Medellín, COL

Corresponding author: Carlos Aníbal Restrepo Bravo, carestrepo@ces.edu.co

Review began 09/24/2026
Review ended 10/15/2026
Published 10/27/2026

© **Copyright** 2026
Contreras López et al. This is an open access article distributed under the terms of the Creative Commons Attribution License CC-BY 4.0., which permits unrestricted use, distribution, and reproduction in any medium, provided the original author and source are credited.

DOI: 10.7759/cureus.118691

Abstract

The subcallosal cingulate (SCC/sgACC) is a proposed target for deep brain stimulation (DBS) in treatment-resistant depression (TRD), and intraoperative local field potentials (LFPs) are being explored as a source of candidate biomarkers.

We report a 52-year-old woman with early-onset, highly refractory TRD and comorbid obsessive-compulsive and anxiety disorders who underwent tractography-guided multitarget DBS with four 8-contact non-directional leads: two in the SCC and two along a trajectory through the posterior-ventral nucleus accumbens (NAc), the anterior bed nucleus of the stria terminalis (BNST), and the anterior limb of the internal capsule (ALIC). In this exploratory technical observation, LFPs were recorded from the macrocontact of a microelectrode in the left SCC of the awake patient, with stimulation OFF, during two music trials: one with a no-music baseline, two neutral songs (rock and classical), and her favorite (happy) song, and one with a baseline and a sad song. Spectra (Welch's method) and aperiodic exponents were compared post hoc, and broadband (3-45 Hz) power during each song was expressed relative to the baseline of the same trial.

Verification of the raw data identified non-neural features that could mimic affective effects: the exported segments had been downsampled without anti-alias filtering, so 60-Hz mains interference appeared as narrow lines at 40 and 20 Hz, and 23 corrupted samples in the first 4 s of the happy-song segment inflated its power more than 200-fold. After their exclusion, broadband power relative to baseline was higher during the sad song (1.43-fold) than during the happy song (0.69-fold; between-song ratio 2.06, permutation p=0.024) and the rock song (0.57-fold; ratio 2.48, p=0.004), but not the classical piece (1.13-fold; p=0.45). Absolute power did not differ between the sad and happy songs, power rose transiently before the sad song began and remained elevated after it ended, and aperiodic exponents showed no valence-related pattern. Three months after stimulation onset, the 17-item Hamilton Depression Rating Scale score decreased from 26 to 13 and the Hamilton Anxiety Rating Scale score from 19 to 8.

This single-case observation provides, at most, a weak post hoc signal of valence-related SCC broadband activity and mainly shows how acquisition and export artifacts can mimic affective LFP effects. Raw-data verification, anti-alias filtering, and repeated, counterbalanced conditions are prerequisites for evaluating intraoperative SCC LFPs as candidate biomarkers.

Categories: Psychiatry, Psychology, Neurosurgery
Keywords: deep brain stimulation, intraoperative local field potentials, multimodal targeting, spectral biomarkers, treatment-resistant depression

Introduction

Major depressive disorder is among the leading causes of disability worldwide, and depressive disorders account for the largest share of disability-adjusted life-years attributable to mental disorders [1]. In the Sequenced Treatment Alternatives to Relieve Depression (STAR*D) trial, cumulative remission after up to four sequential treatment steps was approximately 67%, with lower remission and higher relapse rates among patients who required more steps [2], leaving a substantial group of patients with treatment-resistant depression (TRD).

Deep brain stimulation (DBS) of the subcallosal cingulate (SCC/Brodmann area 25) was introduced on the basis of the metabolic hyperactivity of this region in depression and its reduction with successful antidepressant treatment [3,4]. Open-label series reported sustained responses, but the multicenter, sham-

controlled BROADEN trial did not demonstrate superiority of active over sham stimulation during its six-month blinded phase [5]. A recent pooled analysis of 172 implanted patients reported response and remission rates of approximately 55% and 40%, respectively, at 24 months, with an adverse-event profile consistent with other DBS indications [6]. Tractography studies showed that clinical response depends on engaging a convergence of the forceps minor, uncinate fasciculus, cingulum bundle, and descending subcortical fibers, supporting patient-specific, connectomic targeting [7]. In parallel, nodes of the reward and threat circuitry, such as the nucleus accumbens (NAc) and the bed nucleus of the stria terminalis (BNST), have been explored as alternative or complementary DBS targets [8,9].

Because DBS programming in TRD remains largely empirical, electrophysiological biomarkers are being pursued. Most derive from local field potentials (LFPs), the summed electrical activity of neuronal populations near the recording contact, whose power spectral density (PSD) describes how signal power is distributed across frequencies. The PSD combines narrowband oscillations with a broadband aperiodic (1/f) background, whose power decreases with frequency and whose steepness is summarized by the aperiodic exponent (β). In chronic SCC recordings, changes in the right-hemisphere 1/f slope accompanied treatment response [10], and SCC spectral dynamics tracked individual recovery trajectories in sensing-enabled cohorts [11]; intraoperatively, a decrease in left SCC beta power predicted rapid antidepressant effects [12], and an amygdala gamma-band biomarker has been used to trigger closed-loop ventral capsule/ventral striatum stimulation [13]. Because the aperiodic exponent has been linked to excitation-inhibition balance [14], it must be separated from narrowband oscillations to avoid misattributing broadband shifts to oscillatory changes [15,16]; gamma-band activity has also been proposed as a candidate biomarker of depression [17].

Music offers a naturalistic and reproducible means of engaging these circuits. Music-evoked emotions modulate activity in the amygdala, NAc, hypothalamus, hippocampus, insula, cingulate, and orbitofrontal cortex [18], and intensely pleasurable music elicits dopamine release in the striatum [19]. Happy and sad music recruit partly dissociable limbic-cortical networks [20,21], and individuals with depression preferentially select sad music, a choice that may reflect emotion-regulation goals that maintain negative mood [22]. Of direct relevance to the SCC, transient sadness increases subgenual cingulate activity in healthy volunteers, whereas clinical recovery is accompanied by its reduction [23], and SCC DBS reduces automatic attentional bias toward negative self-referential material in patients with TRD [24].

To our knowledge, intraoperative SCC LFP activity during emotion-evoking music has not been described in TRD. This report is an exploratory technical observation: we describe the verification of intraoperative SCC LFPs recorded during music listening and a post hoc comparison of broadband activity, relative to the preceding no-music baseline, between a sad song and neutral and happy music. Given the involvement of the SCC in negative mood [23], the sad song was the condition of primary interest; however, because each song was presented once, in a fixed order, and without valence or arousal ratings, the design cannot test a sadness-specific SCC response. Broadband power (the integral of the PSD over 3-45 Hz, which equals the variance of the band-limited signal) and the aperiodic exponent were examined descriptively, and all comparisons were defined after the recordings had been obtained. Because verification of the raw recordings revealed acquisition and export artifacts capable of mimicking affective effects, the report also describes how these artifacts were identified. The observation is not intended to establish a biomarker or a clinical phenotype.

Case Presentation

History and presentation

A 52-year-old woman presented with severe, recurrent major depressive disorder that began at approximately 26 years of age, with persistently depressed mood, daily sadness and frequent crying, marked anhedonia, hopelessness, feelings of worthlessness, pathological guilt, progressive loss of motivation, constant rumination, persistent fatigue, and insomnia alternating with hypersomnia. The course was chronic, fluctuating, and progressively refractory, with multiple severe relapses and repeated hospitalizations. She had persistent suicidal ideation and passive death wishes, with two serious suicide attempts (one requiring intensive care) and one aborted attempt, and she had repeatedly expressed a wish for euthanasia. Comorbidities included severe early-onset obsessive-compulsive disorder (contamination, order, and cleanliness obsessions; washing and disinfection rituals; intrusive guilt-related thoughts; and pathological perfectionism) that worsened in parallel with depression, a comorbid anxiety disorder, and chronic insomnia; affective symptoms also worsened during menses. On mental status examination, she was alert, oriented, and cooperative, with profoundly depressed affect and thought content dominated by guilt, hopelessness, and death ideation, without psychotic symptoms; insight was partial and reality testing was preserved.

Treatment resistance was documented after more than 15 psychotropic medications from different classes (selective serotonin reuptake inhibitors, serotonin-norepinephrine reuptake inhibitors, tricyclic antidepressants, mood stabilizers, atypical antipsychotics, benzodiazepines, and glutamatergic modulators), electroconvulsive therapy since diagnosis, intravenous ketamine, repetitive transcranial magnetic stimulation, and prolonged psychotherapy including intensive cognitive-behavioral therapy, all without sustained response or with significant intolerance. Given the extreme treatment resistance, high suicide

risk, chronicity, and absence of conventional alternatives, the interdisciplinary psychiatry-functional neurosurgery team considered her a candidate for DBS. A multitarget approach was chosen according to her symptom profile: the SCC to modulate mood regulation and the dominant depressive network; the BNST to address sustained anxiety, anticipatory fear, and hypervigilance; and the ALIC and adjacent ventral striatum to address obsessive-compulsive symptoms, rumination, and fronto-striatal regulation [3,8,9]. The patient and her family were informed of the investigational nature, risks, benefits, and alternatives of the procedure, and the patient completed and signed written informed consent for surgery, the intraoperative research recordings, and publication. The study was approved by the Ethics Committee of the International Neuromodulation Center (NEMOD).

Operative planning and targeting

Neurosurgical planning specified 3-T MRI (1-mm isotropic contrast-enhanced T1, T2, 3D fluid-attenuated inversion recovery (FLAIR), and 32-40-direction diffusion tensor imaging (DTI)) for tractography-guided SCC targeting [5]. Hardware used was a Vercise Genus P32 non-rechargeable IPG with four long 8-contact non-directional leads (Boston Scientific, Marlborough, MA, USA; bilateral SCC and bilateral NAc-BNST-ALIC) and extensions.

Conventional SCC targeting was performed using standard stereotactic coordinates: X = 7 mm lateral, Y = 8 mm anterior to the anterior commissure (AC), and Z = 2 mm inferior to the midpoint of the AC-PC plane. From this nominal point, the trajectory was adjusted toward the zone of maximal fiber-density convergence, specifically the intersection of the short frontal fibers, the cingulum bundle, and the uncinate fasciculus, to optimize modulation of the fronto-limbic network. For the accumbens-BNST trajectory, coordinates were set at X = 3 mm lateral, Y = 14 mm anterior to the mid-commissural point (MCP) - positioning the lower contacts posterior to the nucleus accumbens and anterior to the BNST - with Z = 2 mm inferior to the MCP. The entry angle was deliberately aligned along the direction of the thalamic radiations, ensuring that the most superior contacts would lie within the ALIC, enabling simultaneous engagement of ventral striatal, BNST, and capsular pathways within a single optimized trajectory [6,9]. Postoperative MRI confirmed the two SCC leads anteriorly and the two NAc-BNST-ALIC leads posteriorly. On probabilistic tractography, the SCC leads reached the intersection of the forceps minor, uncinate fasciculus, and anterior cingulum fibers, and the posterior leads traversed the tract through both NAc into the ALIC; volume of tissue activated (VTA) modeling of the ventral SCC contacts showed activation of cingulum and forceps minor fibers (Figure *1*).

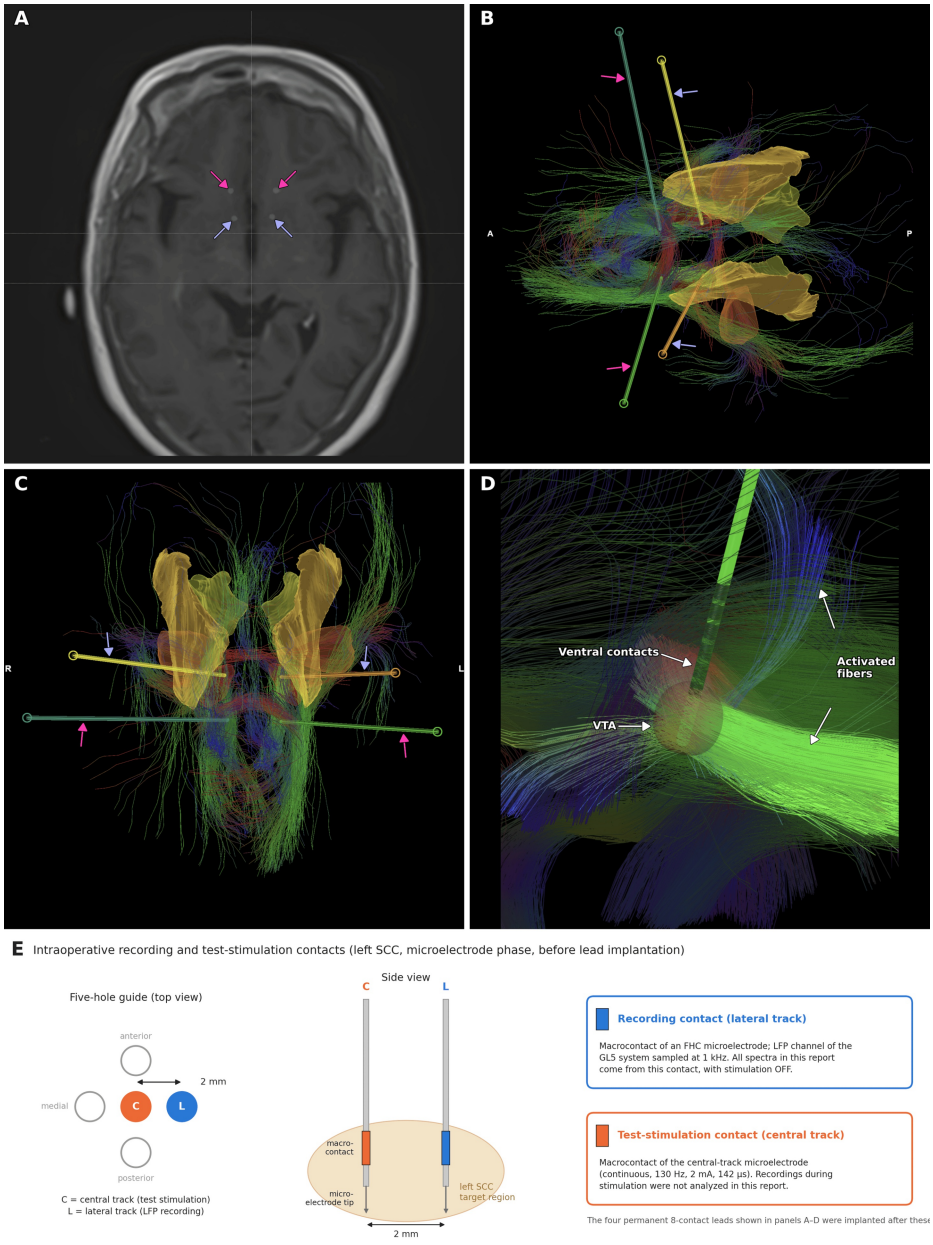


FIGURE 1: Postoperative lead localization, probabilistic tractography, volume of tissue activated (VTA) modeling, and intraoperative recording configuration.

A. Postoperative axial T1-weighted MRI showing the four implanted leads; magenta arrows indicate the two anterior leads in the subcallosal cingulate (SCC), and lavender arrows indicate the two posterior leads along the nucleus accumbens (NAc)-bed nucleus of the stria terminalis (BNST)-anterior limb of the internal capsule (ALIC) trajectory. B. Probabilistic tractography (A, anterior; P, posterior) showing the internal capsule (yellow), the amygdala (orange), and the four leads with the same arrow code: the anterior SCC leads (green and cyan) reach the intersection of the forceps minor, uncinate fasciculus, and anterior cingulum fibers, whereas the posterior leads (orange and yellow) traverse the tract through both NAc and course into the ALIC. C. The same reconstruction rotated so that anterior is at the bottom and posterior at the top (R, right; L, left). D. VTA simulation for the ventral contacts of the SCC lead shown in green, with activation of cingulum and forceps minor fibers (white arrows); the simulation (5 mA, 130 Hz, 90-µs pulse width) illustrates the relationship between the active contacts and these tracts. All targets were implanted with long 8-contact non-directional leads (Boston Scientific, Marlborough, MA, USA). E. Schematic of the intraoperative recording configuration in the left SCC during the microelectrode phase, before lead implantation: LFPs were recorded from the macrocontact of the microelectrode in the lateral track (blue), 2 mm from the central track, whose macrocontact (orange) was used for test stimulation (130 Hz, 2 mA, 142 µs); recordings obtained during stimulation were not analyzed. The schematic is not to scale.

Microelectrode recording (MER) and intraoperative LFP acquisition were performed using the Guideline 5 (GL5) neuromodulation system from FHC (Bowdoin, ME, USA), which provides simultaneous micro- and

low-frequency electrophysiological recording channels. Multitarget surgical planning was carried out using the Brainlab planning environment (Brainlab, Munich, Germany), incorporating its Elements Fibertracking and tractography modules to reconstruct patient-specific white-matter pathways, visualize frontal-limbic tracts, and optimize trajectory selection based on probabilistic tractography [9].

Intraoperative LFP methods

Experimental Design

Recordings were obtained during the microelectrode-recording phase of surgery, before implantation of the definitive leads, with the patient fully awake under local anesthesia and a single low dose of dexmedetomidine. Using the GL5 system, LFPs were recorded at the left SCC target (the first hemisphere operated) from the macrocontact of an FHC microelectrode (3-mm tip) placed in a lateral track 2 mm from the central track; test stimulation was delivered through the macrocontact of the central-track microelectrode (continuous, 130 Hz, 2 mA, 142-µs pulse width) (Figure *1E*). Four songs were selected preoperatively with the patient, according to her musical preferences, as pieces that evoked strong emotions [20,21,25]: rock-neutral ("Enter Sandman," Metallica), classical-neutral (Adagio for Strings, Op. 11, Samuel Barber, conducted by Leonard Bernstein), favorite ranchera-happiness ("Coqueta," Heredero), and ballad-sadness ("Mi viejo," Piero). Emotional labels were based on her preoperative report; intraoperative valence or arousal ratings were not obtained. With stimulation OFF, two continuous trials were recorded (Figure *2A*). Trial 1 (270 s) consisted of a no-music baseline (0-27 s), the rock song (27-83 s), a second baseline (83-117 s), the classical piece (117-170 s), a third baseline (170-200 s), and the happy song (200-270 s). Trial 2 (70.7 s) consisted of a no-music baseline (0-21 s), the sad song (21-51 s), and a no-music period (51-70.7 s). Transitions were marked by tapping the recording cable, which produced a brief mechanical artifact used for segmentation. The protocol was then repeated during test stimulation; these recordings were not analyzed because the exported files could not be verified against the native recordings (they had been exported in a different format, lacked a baseline segment of their own, and contained no identifiable stimulation artifact). This report is therefore restricted to recordings obtained without stimulation.

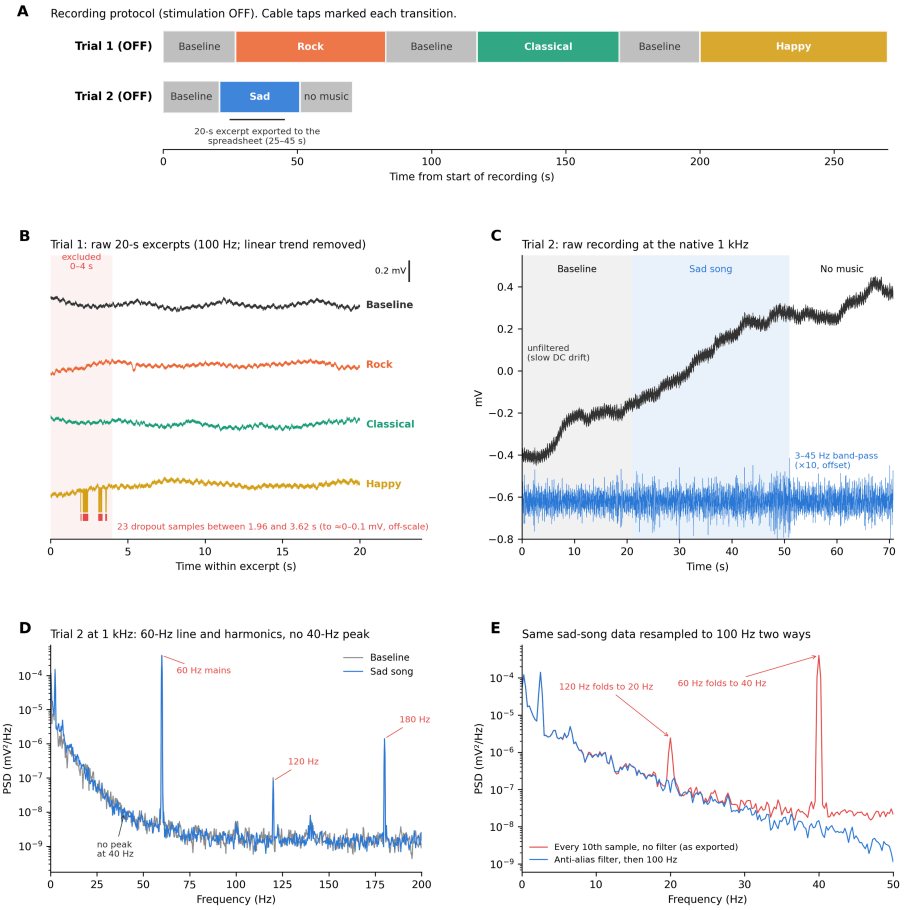


FIGURE 2: Recording protocol, raw local field potentials, and non-neural signal features (stimulation OFF).

A. Timeline of the two trials recorded without stimulation; transitions were marked by cable taps. The bar under trial 2 marks the exported 20-s excerpt (25-45 s), which matched every 10th sample of the native recording. B. Raw 20-s excerpts of trial 1 at 100 Hz (linear trend removed for display). The happy-song excerpt contains 23 corrupted samples between 1.96 and 3.62 s (red ticks; values fall to ≈0-0.1 mV and are clipped in the display); the first 4 s of every trial-1 excerpt (shaded) were excluded from analysis. C. Native 1-kHz recording of trial 2 (black, unfiltered, showing slow DC drift) and the same signal band-pass filtered at 3-45 Hz (blue, ×10, offset). D. Power spectral density (PSD) of trial 2 at 1 kHz, showing a 60-Hz mains line with harmonics and no peak at 40 Hz. E. The sad-song period downsampled to 100 Hz by taking every 10th sample without filtering, as in the exported files (red), and after anti-alias filtering (blue); the 60-Hz and 120-Hz lines fold to 40 and 20 Hz only without filtering. PSDs were estimated with Welch's method (4-s Hann windows, 50% overlap).

Data Verification and Preprocessing

The LFP channel was acquired at 1 kHz and exported as text. For trial 1, the available data were 20-s excerpts exported at 100 Hz (one from a baseline period and one from each song); for trial 2, the complete recording at 1 kHz was available. Before analysis, the data were verified in three steps. First, the exported 20-s excerpt of the sad song was located within the native trial-2 recording by cross-correlation; it matched samples 25-45 s exactly (r = 1.000) when every 10th sample was taken, showing that the exported files had been downsampled by sample decimation without an anti-alias filter, a procedure that folds activity above the new Nyquist frequency (50 Hz) into the analysis band [26]. Second, the spectrum of the native recording was examined up to 500 Hz for line noise. Third, each excerpt was screened for corrupted samples (deviation of more than 0.3 mV from an 11-sample running median) and for slow drift. Because corrupted samples were confined to the first 4 s of one excerpt (see Results), all trial-1 analyses used the 4-20-s window of each excerpt. To keep processing identical across trials, the trial-2 recording was decimated in the same way (every 10th sample) for the main analysis, and the result was checked after anti-alias (finite impulse response) filtering and downsampling. No notch filter was applied, and electrode impedance values were not available.

Spectral Analysis and Post Hoc Statistics

PSDs were estimated with Welch's method (Hann window, 4-s segments, 50% overlap, density scaling, linear detrending; 0.25-Hz resolution) [27,28]. Broadband power was obtained as the integral of the PSD over 3-45 Hz, which, by Parseval's theorem, equals the variance of the band-limited signal and indexes local population activity [29]; bins at 2-3 Hz, 19.5-20.5 Hz, and 39.5-40.5 Hz, which contained narrow lines of non-neural origin, were excluded. The aperiodic exponent (β) was estimated by spectral parameterization (Fitting Oscillations and One-Over-F (FOOOF)/specparam, version 1.1; fixed aperiodic mode, 2-45 Hz) [15,16]. For each song, broadband power was expressed relative to the baseline of the same trial; for trial 2, both the 30-s sad-song period and a 16-s window matched in length to the trial-1 windows (29-45 s) were analyzed. All statistical comparisons were defined after inspection of the data and are therefore post hoc and exploratory. Each condition was divided into non-overlapping 2-s epochs, and broadband power was computed for each epoch. Song-versus-baseline differences were tested with a permutation test on the mean log epoch power (20,000 permutations) [30]. Differences between songs were tested on the song-to-baseline ratio, permuting song and baseline labels within each trial, so that the variability of both baselines was taken into account. Because adjacent epochs are not independent and each song was presented once, p values are reported uncorrected as descriptive measures; Holm-adjusted values are also given for the three contrasts involving the sad song [31].

Results

Intraoperative Results

Raw-data verification: Three non-neural features were identified (Figure *2*). First, the native 1-kHz recording contained a large 60-Hz mains line, which accounted for about 64% of total signal power, with harmonics up to 480 Hz, but no peak at 40 Hz (Figure *2D*). Because the exported data had been downsampled to 100 Hz without anti-alias filtering, the 60-Hz line and its 120-Hz harmonic folded to 40 Hz and 20 Hz, where they appeared in every condition, including the baselines, as narrow lines more than 8,000-fold above neighboring frequencies; after anti-alias filtering, the 40-Hz line disappeared (Figure *2E*). The ≈40-Hz and ≈20-Hz lines are therefore aliased mains interference, and neither their height nor their width carries neural information. In addition, a narrow line at 2.5 Hz, of unidentified and presumably instrumental origin, was present in all conditions at the native sampling rate. Second, the happy-song excerpt contained 23 corrupted samples between 1.96 and 3.62 s, which dropped to ≈0-0.1 mV from a signal level of ≈1.1 mV (Figure *2B*). When these 4 s were included, 3-45-Hz power of the excerpt was ≈218-fold that of its baseline and the spectrum flattened (aperiodic exponent 0.50, R^2=0.66); after their exclusion, the excerpt was comparable to the other conditions (exponent 2.07, R^2=0.93). No corrupted samples were found in the other excerpts or in trial 2. Third, the signal showed a slow DC drift (≈0.8 mV over 70 s in trial 2; Figure *2C*), which was removed by linear detrending and does not affect the 3-45-Hz band.

Song-related changes in broadband power (stimulation OFF): Within trial 1, broadband power relative to baseline was 0.57-fold during the rock song (permutation p=0.024), 1.13-fold during the classical piece (p=0.60), and 0.69-fold during the happy song (p=0.14) (Figure *3A*, *3C*). Within trial 2, it was 1.43-fold during the sad song (p=0.087; 1.31-fold, p=0.21, in the length-matched window) and 1.21-fold after the song ended (p=0.32) (Figure *3B*, *3C*). In the native 1-kHz time course, power had already increased transiently during the last 5 s of the baseline, before the sad song started, and remained elevated after the song ended, without a difference between the song and the subsequent no-music period (ratio 0.98) (Figure *3D*). Repeating the trial-2 analysis with anti-alias filtering instead of sample decimation gave nearly identical results (whole-window ratio 1.59 vs 1.56).

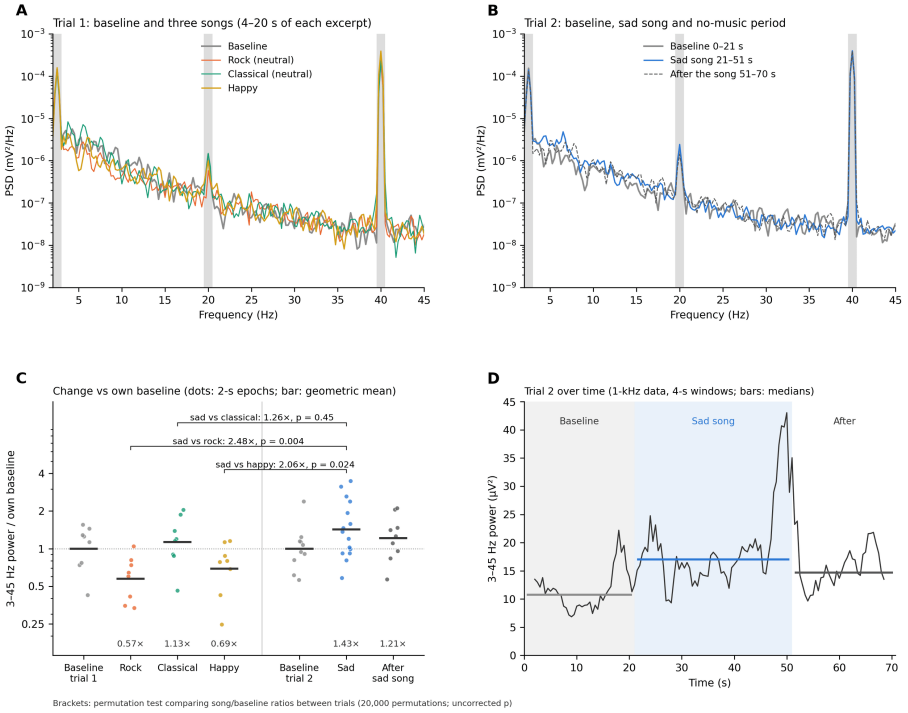


FIGURE 3: Broadband spectral power during each song relative to the baseline of the same trial (stimulation OFF).

A. Power spectral densities (PSDs) of trial 1: baseline, rock, classical, and happy excerpts (4-20 s of each 20-s excerpt). B. PSDs of trial 2: baseline (0-21 s), sad song (21-51 s), and no-music period (51-70 s), downsampled as in trial 1. Grey bands mark the narrow non-neural lines (2.5 Hz, and 60-Hz and 120-Hz mains interference aliased to 40 and 20 Hz) excluded from broadband power. C. 3-45-Hz power of 2-s epochs relative to the geometric mean of the baseline of the same trial; bars show geometric means. Brackets give the ratio between song-to-baseline ratios and the uncorrected permutation p value (20,000 permutations, labels permuted within trials). D. Time course of 3-45-Hz power in trial 2 at 1 kHz (4-s windows, 0.5-s steps); horizontal bars show medians. All analyses are post hoc.

Comparison between songs: Because each song was referred to its own baseline, differences between songs were evaluated on the song-to-baseline ratios. The ratio for the sad song was 2.06-fold that for the happy song (p=0.024; 1.90-fold, p=0.051, in the length-matched window) and 2.48-fold that for the rock song (p=0.004), but did not differ from that for the classical piece (1.26-fold, p=0.45) (Figure *3C*). After Holm adjustment for the three sad-song contrasts, p values were 0.012 (rock), 0.048 (happy), and 0.45 (classical). These contrasts depend on the reference baseline: the two baselines differed in absolute power (22.0 μV^2 in trial 1 vs 12.5 μV^2 in trial 2; p=0.035), and absolute broadband power did not differ between the sad and happy songs (19.5 vs 15.4 μV^2; p=0.26).

Aperiodic exponents ranged from 1.80 to 2.34 across conditions (baselines 2.34 and 1.96; rock 2.04, classical 2.10, happy 2.07, sad 2.04, after the sad song 1.80), without a pattern related to emotional valence. Periodic components fitted by spectral parameterization were small and inconsistent across conditions and were not interpreted.

Postoperative/Early Outcome

Depressive and anxiety symptoms were rated with the 17-item Hamilton Depression Rating Scale (HDRS-17) [32] and the Hamilton Anxiety Rating Scale (HAM-A) [33] before surgery and three months after stimulation was activated. The HDRS-17 total score decreased from 26 to 13 (50%), with the largest item changes in depressed mood (4 to 1), suicidal ideation (3 to 1), work and activities (3 to 1), and genital symptoms (2 to 0), whereas guilt increased from 0 to 1. The HAM-A total score decreased from 19 to 8 (58%), with reductions in mood, cognitive, gastrointestinal, autonomic, and sleep items (Figure *4A*-*4C*). In addition, patient-reported ratings on 11 non-validated items (scored 1-10), obtained at baseline and four weeks after stimulation was activated, improved in sleep quality, hope for the future, social and family satisfaction, concentration, gardening, enjoyment of daily activities, and mood, whereas daytime energy decreased (10 to 5) (Figure *4D*); a global well-being index, defined as the mean change across the 11 items after reverse-scoring the two items for which higher scores indicate worse status, increased by 3.73 points. Medication was not changed between stimulation activation and the three-month assessment. No obsessive-compulsive symptom scale

was available. These open-label ratings from two time points describe the clinical course; they cannot establish efficacy or be attributed to a specific target.

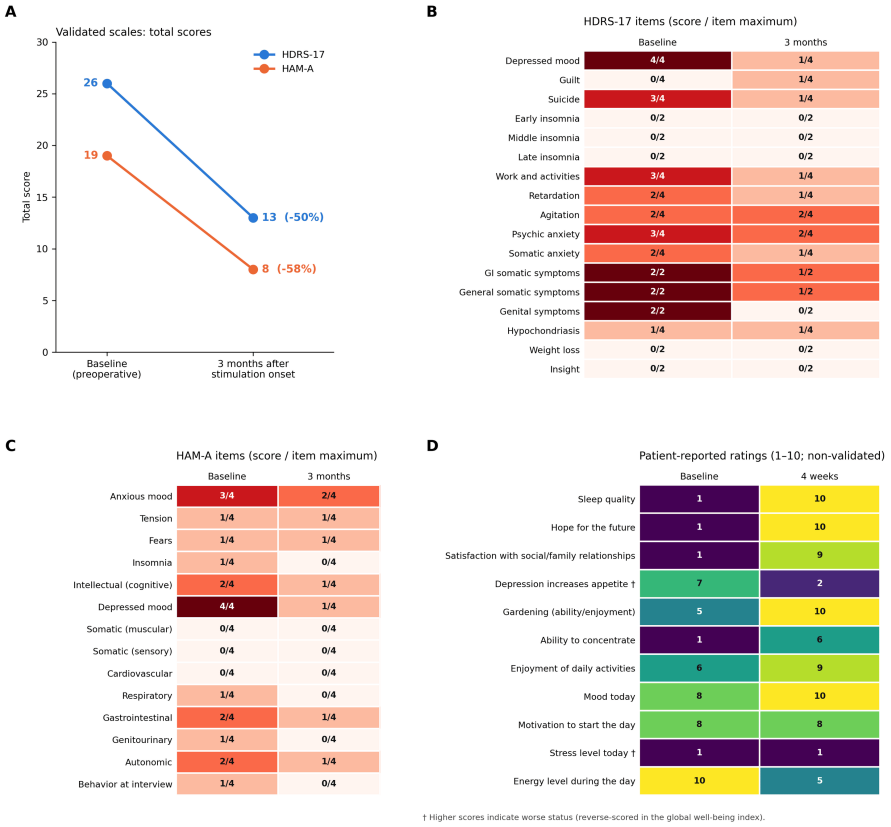


FIGURE 4: Clinical ratings before and after surgery.

A. Total scores of the 17-item Hamilton Depression Rating Scale (HDRS-17)[32] and the Hamilton Anxiety Rating Scale (HAM-A) [33] before surgery and three months after stimulation onset. B, C. Item scores of the HDRS-17 (B) and HAM-A (C), shown as score/item maximum; color intensity is proportional to the fraction of the item maximum. D. Patient-reported ratings (1-10) on 11 non-validated items at baseline and four weeks after stimulation was activated; higher scores indicate more favorable ratings, except for the two items marked †, which were reverse-scored for the global well-being index. Ratings are open-label and descriptive and do not establish treatment efficacy.

Discussion

The main contribution of this report is methodological. Verification of the raw recordings showed that the most conspicuous spectral features of these data were not neural: the ≈40-Hz and ≈20-Hz lines were 60-Hz mains interference and its harmonic folded into the analysis band by downsampling without anti-alias filtering, and the largest broadband change, a more than 200-fold power increase with spectral flattening, arose from 23 corrupted samples in a single excerpt. Each of these features could easily be mistaken for an affective or stimulation-related effect: a 40-Hz peak may be expected in auditory paradigms, because auditory steady-state responses occur at this frequency and depend on arousal, attention, inhibitory tone, and stimulus predictability [34-40], and broadband power shifts and spectral flattening are interpreted as changes in population activity and excitation-inhibition balance [14,29]. In intraoperative recordings, where time is limited and environmental interference is common, inspection of raw traces, analysis at the native sampling rate, and anti-alias filtering before any downsampling should therefore precede spectral interpretation [26].

After these artifacts were excluded, the only signal suggestive of a valence-related effect was that broadband SCC power, relative to the preceding baseline, increased during the sad song and decreased during the happy and rock songs. This direction would be consistent with the increase in subgenual cingulate activity during transient sadness and its reduction with recovery [3,23], with the reduction of attentional bias toward negative self-referential material after SCC DBS [24], and with the close relationship between broadband LFP power and local population spiking [29]. However, several observations argue for caution. The sad-song ratio did not differ from that of the neutral classical piece; the songs were recorded in two separate trials

whose baselines differed in absolute power, so the contrasts depend on the reference used, and absolute power did not differ between the sad and happy songs; and in trial 2 power rose transiently before the song started and remained elevated after it ended, a time course more consistent with a slow change in state, such as arousal or anticipation, than with a response locked to the music. Music modulates deep and cortical field potentials, including beat-related beta synchrony in basal ganglia LFPs and emotion-specific cortical activity patterns [41,42], and standardized musical stimuli remain an attractive way to probe affective circuits intraoperatively, but the present data do not establish a valence-specific SCC response.

The aperiodic exponent reflects excitation-inhibition balance and varies with vigilance state and task engagement [43,44]; event-related changes in the spectral slope track attention and age-related shifts in excitation-inhibition balance and predict behavior [44,45], resting exponents predict cognitive decline and change across the lifespan [46,47], and flatter exponents relate to inefficient information processing [48]. Because the exponent is state-dependent, behavioral state must be documented when it is used as a biomarker. In the present recordings, the exponent varied between 1.80 and 2.34 without a pattern related to the emotional content of the music, and the only marked departure from 1/f scaling was produced by corrupted samples, which shows that an apparently flattened spectrum should prompt inspection of the raw signal before physiological interpretation.

Limitations and future directions

This report has important limitations. First, it describes a single patient and a single intraoperative session, and each song was presented once, in a fixed order, without repetition, randomization, or counterbalancing; differences between songs may therefore reflect acoustic features, familiarity, preference, time, or arousal rather than emotional valence, and no intraoperative valence or arousal ratings were obtained. Second, the sad song was recorded in a different trial from the other songs, with a baseline that differed in absolute power, so between-song contrasts depend on the reference baseline. Third, for trial 1 only 20-s excerpts exported at 100 Hz without anti-alias filtering were available; aliased components could not be removed retrospectively and were handled by excluding the affected frequency bins. Fourth, all statistical comparisons were post hoc, epochs within a condition are not independent, and p values are descriptive. Fifth, non-neural contributions such as muscle or movement activity cannot be excluded without simultaneous electromyography or video, and the source of the 2.5-Hz line was not identified. Sixth, recordings during test stimulation were not analyzed because the exported files could not be verified, so no inference about the effect of stimulation on SCC activity can be drawn. Finally, the clinical outcomes were open-label, were obtained at two time points, did not include an obsessive-compulsive symptom scale, and reflect chronic multitarget stimulation, so they cannot be related to the intraoperative observations. Future intraoperative studies should record at the native sampling rate with anti-alias filtering, include a no-stimulus reference recording, verify raw traces before analysis, present repeated and counterbalanced stimuli with concurrent valence ratings, and prespecify the analyses.

Conclusions

In this exploratory single-case technical observation, verification of intraoperative SCC LFPs recorded during emotion-evoking music showed that the most salient spectral features, a 40-Hz line and a large broadband increase with spectral flattening, arose from aliased mains interference and corrupted samples rather than from neural activity. After their exclusion, broadband power increased relative to baseline during the sad song and decreased during the happy and rock songs, a post hoc signal that did not distinguish the sad song from a neutral classical piece and was not time-locked to the music. These findings do not establish a valence-related SCC biomarker; they indicate that raw-data verification, anti-alias filtering, and repeated, counterbalanced conditions are prerequisites for evaluating intraoperative SCC LFPs as candidate biomarkers for personalized DBS.

Additional Information

Author Contributions

All authors have reviewed the final version to be published and agreed to be accountable for all aspects of the work.

Concept and design: William O. Contreras López, Carlos Aníbal Restrepo Bravo

Acquisition, analysis, or interpretation of data: William O. Contreras López, Carlos Aníbal Restrepo Bravo

Drafting of the manuscript: William O. Contreras López, Carlos Aníbal Restrepo Bravo

Critical review of the manuscript for important intellectual content: William O. Contreras López, Carlos Aníbal Restrepo Bravo

Supervision: William O. Contreras López

Disclosures

Human subjects: Informed consent for treatment and open access publication was obtained or waived by all participants in this study. Research Ethical Board of Hospital Internacional de Colombia, Bucaramanga-Santander, Colombia issued approval N/A. All procedures were conducted in accordance with institutional guidelines, national regulations, and the principles outlined in the Declaration of Helsinki. **Conflicts of interest:** In compliance with the ICMJE uniform disclosure form, all authors declare the following: **Payment/services info:** All authors have declared that no financial support was received from any organization for the submitted work. **Financial relationships:** All authors have declared that they have no financial relationships at present or within the previous three years with any organizations that might have an interest in the submitted work. **Other relationships:** All authors have declared that there are no other relationships or activities that could appear to have influenced the submitted work.

References

1. Global, regional, and national burden of 12 mental disorders in 204 countries and territories, 1990-2019: a systematic analysis for the Global Burden of Disease Study 2019. Lancet Psychiatry. 2022, 9:137-50. 10.1016/S2215-0366(21)00395-3
2. Rush AJ, Trivedi MH, Wisniewski SR, et al.: Acute and longer-term outcomes in depressed outpatients requiring one or several treatment steps: a STAR*D report. Am J Psychiatry. 2006, 163:1905-17. 10.1176/ajp.2006.163.11.1905
3. Mayberg HS, Lozano AM, Voon V, et al.: Deep brain stimulation for treatment-resistant depression . Neuron. 2005, 45:651-60. 10.1016/j.neuron.2005.02.014
4. Lozano AM, Mayberg HS, Giacobbe P, Hamani C, Craddock RC, Kennedy SH: Subcallosal cingulate gyrus deep brain stimulation for treatment-resistant depression. Biol Psychiatry. 2008, 64:461-7. 10.1016/j.biopsych.2008.05.034
5. Holtzheimer PE, Husain MM, Lisanby SH, et al.: Subcallosal cingulate deep brain stimulation for treatment-resistant depression: a multisite, randomised, sham-controlled trial. Lancet Psychiatry. 2017, 4:839-49. 10.1016/S2215-0366(17)30371-1
6. Himes LM, Mayberg HS, Husain MM, et al.: Revisiting subcallosal cingulate deep brain stimulation for depression: long-term safety and effectiveness outcomes from a pooled analysis of 172 implanted patients. Brain Stimul. 2025, 18:1632-40. 10.1016/j.brs.2025.08.017
7. Riva-Posse P, Choi KS, Holtzheimer PE, et al.: Defining critical white matter pathways mediating successful subcallosal cingulate deep brain stimulation for treatment-resistant depression. Biol Psychiatry. 2014, 76:963-9. 10.1016/j.biopsych.2014.03.029
8. Bewernick BH, Hurlemann R, Matusch A, et al.: Nucleus accumbens deep brain stimulation decreases ratings of depression and anxiety in treatment-resistant depression. Biol Psychiatry. 2010, 67:110-6. 10.1016/j.biopsych.2009.09.013
9. Ye K, Cao Y, Wu Y, et al.: Therapeutic deep brain stimulation targeting BNST-NAc circuit driven large-scale brain networks in treatment-resistant depression. Transl Psychiatry. 2025, 15:442. 10.1038/s41398-025-03669-w
10. Veerakumar A, Tiruvadi V, Howell B, et al.: Field potential 1/f activity in the subcallosal cingulate region as a candidate signal for monitoring deep brain stimulation for treatment-resistant depression. J Neurophysiol. 2019, 122:1023-35. 10.1152/jn.00875.2018
11. Alagapan S, Choi KS, Heisig S, et al.: Cingulate dynamics track depression recovery with deep brain stimulation. Nature. 2023, 622:130-8. 10.1038/s41586-023-06541-3
12. Sendi MS, Waters AC, Tiruvadi V, et al.: Intraoperative neural signals predict rapid antidepressant effects of deep brain stimulation. Transl Psychiatry. 2021, 11:551. 10.1038/s41398-021-01669-0
13. Scangos KW, Khambhati AN, Daly PM, et al.: Closed-loop neuromodulation in an individual with treatment-resistant depression. Nat Med. 2021, 27:1696-700. 10.1038/s41591-021-01480-w
14. Gao R, Peterson EJ, Voytek B: Inferring synaptic excitation/inhibition balance from field potentials . Neuroimage. 2017, 158:70-8. 10.1016/j.neuroimage.2017.06.078
15. Donoghue T, Haller M, Peterson EJ, et al.: Parameterizing neural power spectra into periodic and aperiodic components. Nat Neurosci. 2020, 23:1655-65. 10.1038/s41593-020-00744-x
16. Gerster M, Waterstraat G, Litvak V, et al.: Separating neural oscillations from aperiodic 1/f activity: challenges and recommendations. Neuroinformatics. 2022, 20:991-1012. 10.1007/s12021-022-09581-8
17. Fitzgerald PJ, Watson BO: Gamma oscillations as a biomarker for major depression: an emerging topic . Transl Psychiatry. 2018, 8:177. 10.1038/s41398-018-0239-y
18. Koelsch S: Brain correlates of music-evoked emotions. Nat Rev Neurosci. 2014, 15:170-80. 10.1038/nrn3666
19. Salimpoor VN, Benovoy M, Larcher K, Dagher A, Zatorre RJ: Anatomically distinct dopamine release during anticipation and experience of peak emotion to music. Nat Neurosci. 2011, 14:257-62. 10.1038/nn.2726
20. Fuentes-Sánchez N, Espino-Payá A, Prantner S, Sabatinelli D, Pastor MC, Junghöfer M: On joy and sorrow: neuroimaging meta-analyses of music-induced emotion. Imaging Neurosci (Camb). 2025, 3:10.1162/imag_a_00425
21. Mitterschiffthaler MT, Fu CH, Dalton JA, Andrew CM, Williams SC: A functional MRI study of happy and sad affective states induced by classical music. Hum Brain Mapp. 2007, 28:1150-62. 10.1002/hbm.20337
22. Millgram Y, Joormann J, Huppert JD, Tamir M: Sad as a matter of choice? Emotion-regulation goals in depression. Psychol Sci. 2015, 26:1216-28. 10.1177/0956797615583295
23. Mayberg HS, Liotti M, Brannan SK, et al.: Reciprocal limbic-cortical function and negative mood: converging PET findings in depression and normal sadness. Am J Psychiatry. 1999, 156:675-82. 10.1176/ajp.156.5.675
24. Hilimire MR, Mayberg HS, Holtzheimer PE, Broadway JM, Parks NA, DeVylder JE, Corballis PM: Effects of subcallosal cingulate deep brain stimulation on negative self-bias in patients with treatment-resistant depression. Brain Stimul. 2015, 8:185-91. 10.1016/j.brs.2014.11.010

25. Mayberg H, Riva Posse P, Rozell C, et al.: Electrophysiological biomarkers to optimize DBS for depression III. BRAIN Initiative Investigators Meeting. The BRAIN Initiative, Bethesda; 2019.
26. Shannon CE: Communication in the presence of noise. Proc IRE. 1949, 37:10-21. 10.1109/JRPROC.1949.232969
27. Welch P: The use of fast Fourier transform for the estimation of power spectra: a method based on time averaging over short, modified periodograms. IEEE Trans Audio Electroacoust. 1967, 15:70-3. 10.1109/TAU.1967.1161901
28. Harris FJ: On the use of windows for harmonic analysis with the discrete Fourier transform . Proc IEEE Inst Electr Electron Eng. 1978, 66:51-83. 10.1109/proc.1978.10837
29. Manning JR, Jacobs J, Fried I, Kahana MJ: Broadband shifts in local field potential power spectra are correlated with single-neuron spiking in humans. J Neurosci. 2009, 29:13613-20. 10.1523/JNEUROSCI.2041-09.2009
30. Maris E, Oostenveld R: Nonparametric statistical testing of EEG- and MEG-data. J Neurosci Methods. 2007, 164:177-90. 10.1016/j.jneumeth.2007.03.024
31. Holm S: A simple sequentially rejective multiple test procedure . Scand J Stat. 1979, 6:65-70.
32. Hamilton M: A rating scale for depression. J Neurol Neurosurg Psychiatry. 1960, 23:56-62. 10.1136/jnnp.23.1.56
33. Hamilton M: The assessment of anxiety states by rating . Br J Med Psychol. 1959, 32:50-5. 10.1111/j.2044-8341.1959.tb00467.x
34. Galambos R, Makeig S, Talmachoff PJ: A 40-Hz auditory potential recorded from the human scalp . Proc Natl Acad Sci U S A. 1981, 78:2643-7. 10.1073/pnas.78.4.2643
35. Picton TW, John MS, Purcell DW, Plourde G: Human auditory steady-state responses: the effects of recording technique and state of arousal. Anesth Analg. 2003, 97:1396-402. 10.1213/01.ANE.0000082994.22466.DD
36. Picton TW, John MS, Dimitrijevic A, Purcell D: Human auditory steady-state responses. Int J Audiol. 2003, 42:177-219. 10.3109/14992020309101316
37. Matulyte G, Parciauskaite V, Bjekic J, Pipinis E, Griskova-Bulanova I: Gamma-band auditory steady-state response and attention: a systemic review. Brain Sci. 2024, 14:10.3390/brainsci14090857
38. Toso A, Wermuth AP, Arazi A, Braun A, Jong TG, Uhlhaas PJ, Donner TH: 40 Hz steady-state response in human auditory cortex is shaped by GABAergic neuronal inhibition. J Neurosci. 2024, 44:10.1523/JNEUROSCI.2029-23.2024
39. Yokota Y, Tanaka K, Chang M, Naruse Y, Imamura Y, Fujii S: Gamma music: a new acoustic stimulus for gamma-frequency auditory steady-state response. Front Hum Neurosci. 2023, 17:1287018. 10.3389/fnhum.2023.1287018
40. Larsen KM, Thapaliya K, Barth M, Lin CS, Siebner HR, Garrido MI: Phase locking of 40 Hz auditory steady state responses is modulated by sensory predictability and linked to cerebellar myelination. Hum Brain Mapp. 2025, 46:e70178. 10.1002/hbm.70178
41. Sharma V, Saha U, Saha J, Chen R, Thaut M: Intracranial basal ganglia LFP show increases in event-related beta synchrony during beat entrainment of finger movements in Parkinson's disease. J Neurol Sci. 2023, 455:121076. 10.1016/j.jns.2023.121076
42. Putkinen V, Nazari-Farsani S, Seppälä K, et al.: Decoding music-evoked emotions in the auditory and motor cortex. Cereb Cortex. 2021, 31:2549-60. 10.1093/cercor/bhaa373
43. Østergaard FG, Penninx BW, Das N, et al.: The aperiodic exponent of neural activity varies with vigilance state in mice and men. PLoS One. 2024, 19:e0301406. 10.1371/journal.pone.0301406
44. Kałamała P, Gyurkovics M, Bowie DC, et al.: Event-induced modulation of aperiodic background EEG: attention-dependent and age-related shifts in E:I balance, and their consequences for behavior. Imaging Neurosci (Camb). 2024, 2:10.1162/imag_a_00054
45. Deodato M, Melcher D: Aperiodic EEG predicts variability of visual temporal processing. J Neurosci. 2024, 44:10.1523/JNEUROSCI.2308-23.2024
46. Finley AJ, Angus DJ, Knight EL, van Reekum CM, Lachman ME, Davidson RJ, Schaefer SM: Resting EEG periodic and aperiodic components predict cognitive decline over 10 years. J Neurosci. 2024, 44:10.1523/JNEUROSCI.1332-23.2024
47. Leroy S, Bublitz V, von Dincklage F, Antonenko D, Fleischmann R: Normative characterization of age-related periodic and aperiodic activity in resting-state real-world clinical EEG recordings. Front Aging Neurosci. 2025, 17:1540040. 10.3389/fnagi.2025.1540040
48. Ostlund BD, Alperin BR, Drew T, Karalunas SL: Behavioral and cognitive correlates of the aperiodic (1/f-like) exponent of the EEG power spectrum in adolescents with and without ADHD. Dev Cogn Neurosci. 2021, 48:100931. 10.1016/j.dcn.2021.100931